Discharge-Chamber Sputtering in Mercury Ion Thrusters

W. S. Williamson* and J. Hyman Jr.†
Hughes Research Laboratories, Malibu, Calif.

Discharge-chamber sputter erosion has been investigated in two electron-bombardment mercury ion thrusters at 8-cm and 12-cm beam diameter (respectively, the SIT-8 and the SIT-12 thrusters). Sputter erosion is found to be concentrated primarily on the screen electrode and is due primarily to singly charged mercury ions, Hg^+. A model of discharge-chamber sputter-erosion has been developed that predicts erosion rates that are in good agreement with observed rates. A three fold reduction in the rate of total mass erosion has been achieved in both the SIT-8 and SIT-12 thrusters by biasing the thruster shell (including screen electrode) at keeper potential rather than at cathode potential.

Introduction

SPUTTER erosion of discharge-chamber surfaces has been identified as an important life-limiting process in electron-bombardment mercury ion thrusters.[1,2] Present mercury thruster designs incorporate features that reduce the failure hazard posed by sputter erosion[3]; these measures appear to be adequate for small (8-cm-diameter) thrusters, but further improvement is needed in large (30-cm-diameter) thrusters intended for primary-propulsion application. Details of the discharge processes that cause sputter erosion have, however, remained largely unexplored. This paper describes the results of an investigation of discharge-chamber sputter erosion and the development of several analytical and diagnostic tools that have been used to advantage in this investigation. In addition, a straightforward modification in discharge-chamber design is described that has resulted in a three fold reduction in the rate of total mass erosion measured in operation of an 8-cm and a 12-cm mercury ion thruster.

Techniques of Experimental Measurements

The present investigation has followed a strategy that permits direct comparison of measured rates of sputter erosion with the measured intensity of ion-bombardment patterns inside an operating electron-bombardment mercury ion thruster. The extent of ion sputtering is measured directly by visual observation of erosion patterns on multilayer thin metallic films of contrasting color; this technique was reported in a related investigation.[4] The ion-bombardment intensity patterns are determined by a wide variety of experimental techniques including the use of Langmuir probes, wall probes, and an $E \times B$-type ion velocity probe. A computerized model[5] of discharge-chamber processes has also been developed to correlate the separate plasma measurements and to predict the correlation of related variables. The 8-cm satellite-control ion thruster (SIT-8)[6] was chosen as the principal subject for this investigation because it represents the furthest extension of the technology base. Additional measurements were also carried out with the SIT-12 (12-cm beam diameter) ion thruster.[7] All measurement and testing was carried out in the ion thruster diagnostic facility shown in Fig. 1. The test facility is arranged so that the beam of the ion thruster fires downward into a frozen mercury collector, which was installed to avoid the experimental uncertainties that might result from backsputtering of nonvolatile material from a conventional solid-metal collector. Typical facility pressures (with an operating thruster) are in the range of 1 to 5×10^{-4} Pa. Several of the most important diagnostic measurements are described in greater detail in the following.

Langmuir Probes

The electron distribution function of an operating electron-bombardment mercury ion thruster is known to consist of two components[8]: a monoenergetic component, having an energy close to that corresponding to the keeper-to-anode potential difference, and a Maxwellian component, with a temperature of several electron volts. As shown in Fig. 2, Langmuir probes (placed in the SIT-8 discharge) have been employed in this investigation to measure the densities, monoenergetic energy, and Maxwellian temperature of the electron populations. In addition, the plasma potential was measured relative to the thruster shell.

Langmuir-probe data are acquired and reduced by an on-line digital computer and probe-scanning system. To acquire a Langmuir-probe datum set, a 0 to 100 V voltage ramp is applied to the probe tip; during this voltage sweep, 50 current-voltage datum pairs are sampled, digitized, and stored by the automatic system. These data are immediately reduced by a computer algorithm that calculates the five plasma parameters listed earlier. A consistency parameter is also printed out, which indicates the degree to which the data agree with the analytical model employed by the data-reduction algorithm. (Inconsistency can result if, for example, a high-voltage arc occurs in the beam-extraction system during acquisition of the current-voltage datum set.) This entire procedure requires approximately 90 s from ramp initiation to completion of printout.

The Langmuir-probe structure, which is at thruster-shell potential (1.2 kV above ground), can be moved throughout the discharge chamber with controls located outside the vacuum bulkhead. Figure 3a shows a contour plot of the plasma potential in the SIT-8 discharge that was acquired with the Langmuir-probe facility.

Discharge Computer Model

A computer model has been developed that describes the discharge processes by which ion generation and plasma loss occur in an electron-bombardment thruster. This model requires as input measurements of the thruster neutral-mercury efflux (deduced from the discharge propellant-utilization efficiency), the doubly charged ion fraction in the beam (measured with the $E \times B$-type velocity analyzer), and a

Presented as Paper 76-1026 at the AIAA International Electric Propulsion Conference, Key Biscayne, Fla., Nov. 14-17, 1976; submitted Dec. 12, 1977; revision received June 20, 1978.

Index category: Electric and Advanced Space Propulsion.

*Member of Technical Staff, Ion Physics Dept. Member AIAA.

†Head, Plasma Research Section, Ion Physics Dept. Associate Fellow AIAA.

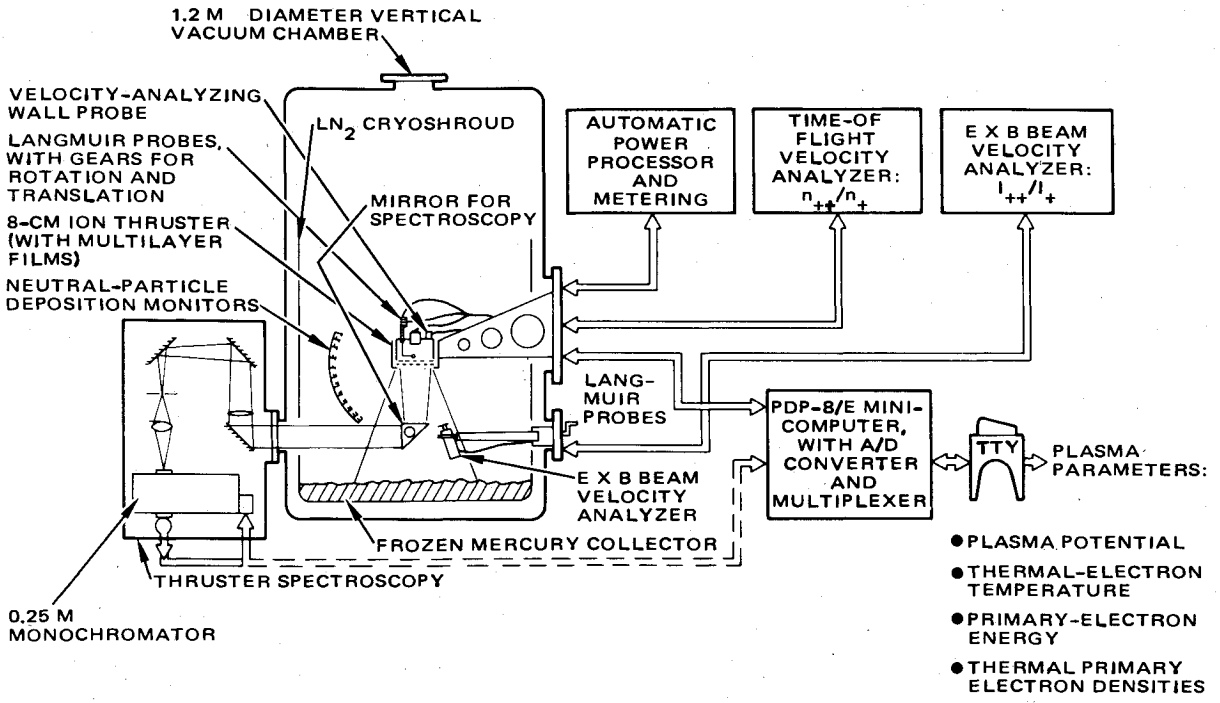

Fig. 1 Ion thruster diagnostic facility.

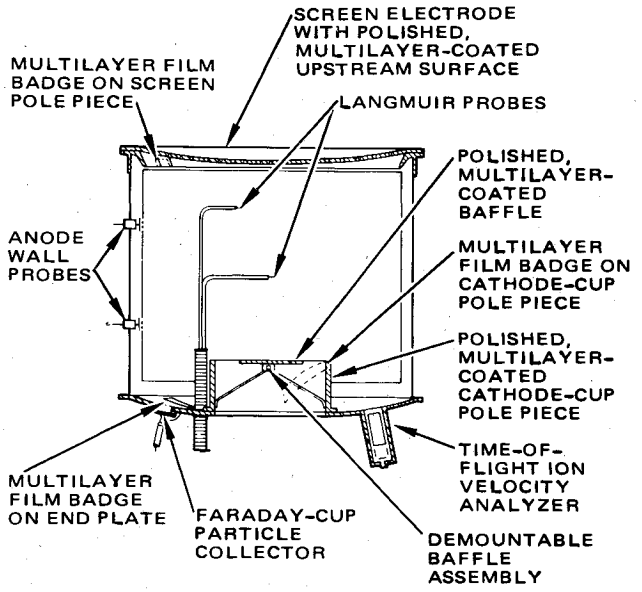

Fig. 2 Thruster-mounted plasma diagnostics.

complete set of Langmuir-probe data. The model employs known cross sections for ionization and excitation to calculate the following output quantities: generation rates of singly and doubly charged mercury ions (Hg^+, Hg^{++}) as functions of position in the discharge, density profiles of neutral mercury (Hg^0) and Hg^{++} ions, and fluxes, Γ_+ and Γ_{++}, of Hg^+ and Hg^{++} ions to all discharge-chamber surfaces.

Figures 3b and 3c display typical results from this model for operation of the SIT-8 thruster; Fig. 3b shows calculated ion-generation rates for singly charged ions (Hg^+), and Fig. 3c shows calculated ion wall currents, compared with currents measured by wall and beam probes.

The discharge computer model does not calculate ion trajectories. Impact energies are therefore not known directly, but an average impact energy can be calculated by weighting plasma potentials at the ion formation site with the generation rates at that location and summing over the appropriate plasma volume.

Laminar-Thin-Film (LTF) Erosion Measurements

Sputter-erosion rates have been measured on discharge-chamber surfaces by applying very thin (50-nm-thick) layers of alternating color-contrasting metals; in these measurements, thin films of molybdenum and copper were used predominantly. These films are applied by a controlled sputter-deposition process, either directly to a polished discharge-chamber surface or to a strip of tantalum shimstock which is then spotwelded to the surface of interest.

When these films (which originally appear homogenous) are exposed to sputter erosion, visible bands of Cu and Mo appear, forming a contour map of the erosion profile. Quantitative measures of the erosion depth by these contours are made by employing a "diagnostic etch" procedure (illustrated in Fig. 4) described as follows: an LTF-covered surface that has been exposed to discharge-chamber sputter erosion is covered by a mask of thin sheet stainless steel. The mask is placed ~1 mm above the surface, and a small aperture in the mask is centered over the region of interest. The sample is then exposed to sputter etching in an argon ion beam until all LTFs have been removed from the region under the mask aperture. This procedure results in the establishment of a gentle gradient in the depth erosion of the LTFs in the region of the sample that lay under the edges of the mask aperture. The gradient in erosion renders the LTF edges visible (with the aid of a microscope) so that the number of film layers remaining can be counted; thus, a quantitative measure of the rate of depth erosion R_{Mo} of the Mo is established.

In Fig. 4, an electron baffle is shown before and after a diagnostic etch has been performed. Before exposure to discharge-chamber sputter erosion, the baffle had been polished, coated with seven layers of Cu and eight layers of Mo (all 50-nm thick), and exposed to sputter-erosion in the SIT-8 thruster discharge. A diagnostic etch was then performed using a straight slot aperture in the etching mask. (The diagnostic-etched region is shown stippled.) In the photomicrograph (upper left-hand corner of Fig. 4), six Cu layers are visible, indicating erosion of 100 nm of Mo and 50 (+50, −0) nm of Cu.

The LTF erosion-measurement method provides an absolute quantitative measure of erosion depth (with a ±25-nm uncertainty of exactly where erosion stopped in an LTF

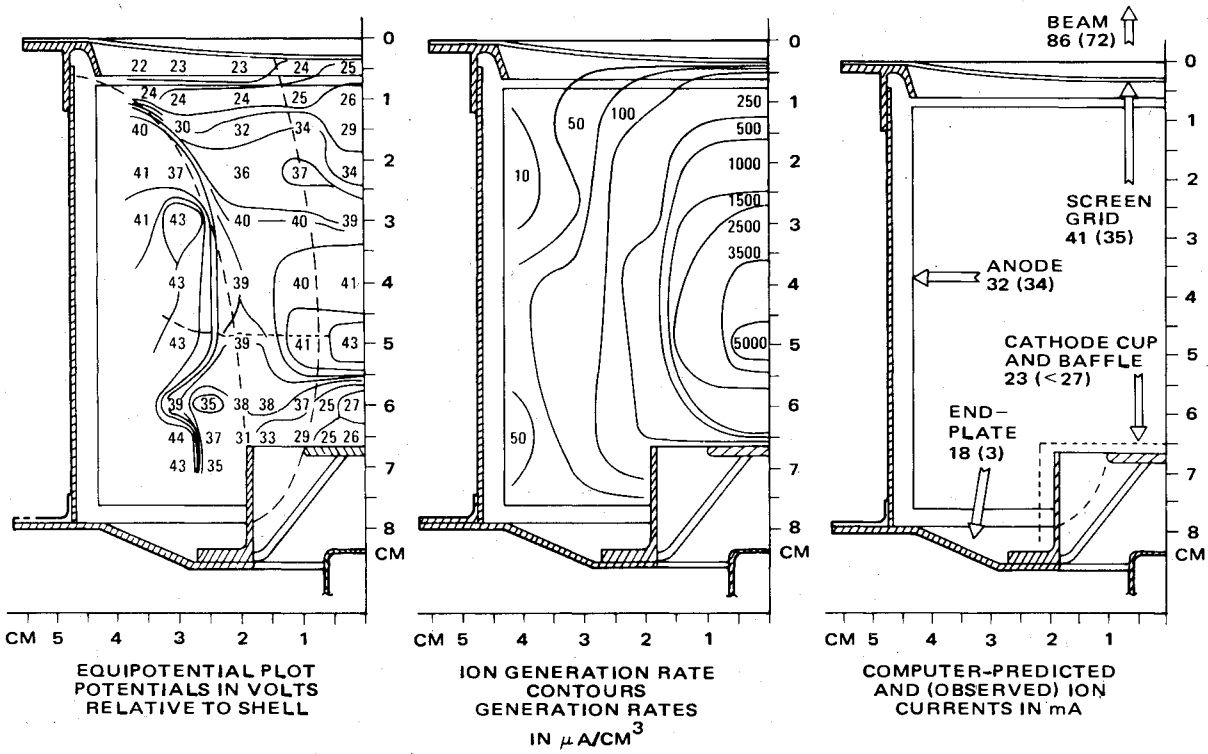

Fig. 3 Discharge plasma properties in the SIT-8.

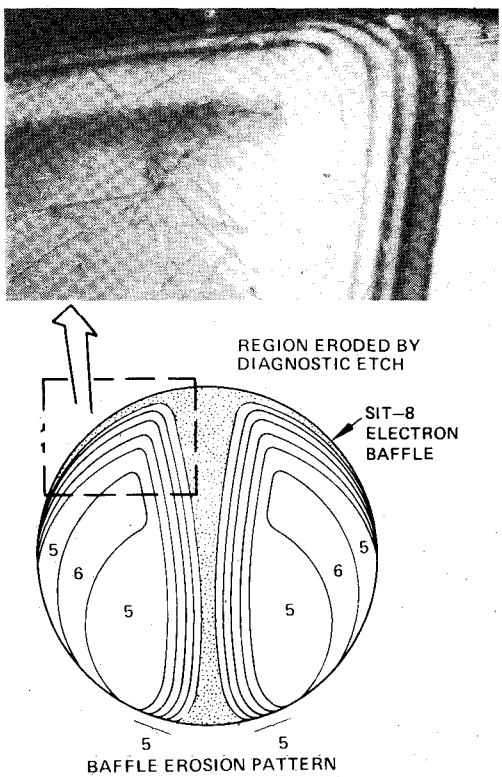

Fig. 4 Diagnostic-etch procedure (numbers indicate copper layers remaining). The photomicrograph (top) shows an enlarged view of the area outlined by the dashed rectangle.

layer), and it is easily implemented in electron-bombardment thrusters. This technique has proven to be of great utility in the present investigation.

Sputter-Erosion Rates and Patterns in the SIT-8 and SIT-12 Thrusters

The rates of sputter erosion on critical discharge-chamber surfaces were measured in the SIT-8 and SIT-12 thrusters. These measurements were accomplished with the LTF/diagnostic-etch technique described earlier; LTF badges were attached to discharge-chamber surfaces by spotwelding, and each thruster was operated on a standard operating point for typically 100 to 200 hours. During thruster operation, the beam was incident on a frozen mercury pool to avoid contamination by nonvolatile backsputtered target material. Results of the erosion tests are presented in Table 1, where the erosion depth per hour is tabulated for each surface studied. These data show that the depth erosion rates and patterns of the SIT-8 and SIT-12 are virtually identical. The most intense erosion occurs over a small surface area on the downstream edge of the cathode-cup polepiece. The screen electrode, however, contributes the overwhelming majority of the eroded mass because of the large surface area involved. Other notable features of the erosion patterns are listed below:

1) The screen electrode is eroded with a high degree of uniformity. Only once in several tests was a very slight degree

Table 1 Measured sputter-erosion rates for SIT-8 and SIT-12

Location of laminar-film badge	Erosion rate, pm/h SIT-8 standard configuration	Erosion rate, pm/h SIT-12 standard configuration
Screen electrode	970-1450	971-1460
Screen polepiece		
Sharp edge	<490	971-1460
Elsewhere	<490	<485
Cathode-cup polepiece		
Inside	<490	<485
Downstream edge	2430-2920	4000-6000
Ridge, downstream on outside	...	1943-2000
Outside	<490	<485
Baffle		
Upstream	<970	<485
Downstream	490-970	<485
Endplate	<970	<485
Total mass erosion rate, μg/h	81	144

Table 2 Erosion-rate estimation in the standard SIT-8

Critical surface	Predicted: Incident flux Γ_+, $m^{-2}\,s^{-1}$	Predicted: Incident flux Γ_{++}, $m^{-2}\,s^{-1}$	Predicted: Mean impact energy $\langle\epsilon\rangle$, eV	Predicted: Erosion rate, R_{Mo}, nm/h	Observed: Erosion rate, R_{Mo}, nm/h
	1.32×10^{20}		40.1	2.25	
Screen electrode		1.66×10^{18}	80.2	0.53	
				2.78	1.21
	9.62×10^{19}		27.3	0.17	
Cathode-cup polepiece/baffle		4.54×10^{18}	54.6	0.32	
				0.49	1.22
	1.95×10^{19}		37.2	0.23	
Endplate		2.91×10^{17}	74.4	0.07	
				0.30	<0.49

of nonuniformity observed; this took the form of a slight enhancement of erosion in a diffuse annular region on a radius of about 20 mm from the thruster axis.

2) Erosion of the electron baffles proceeds at a very slow rate. This observation contrasts with the rapid baffle erosion that has been observed in larger thrusters.[2]

3) In no case was any erosion of the endplate observed.

4) Enhancement of sputter erosion is consistently observed on sharp or projecting surfaces in contact with the discharge plasma. Sharp edges present on the electron baffle, screen polepiece, and cathode-cup polepiece were eroded much more strongly than surrounding surfaces; even a gently rounded ridge on the outside, downstream surface of the SIT-12 cathode-cup polepiece displayed this effect.

Sputter-Erosion Mechanism and Erosion-Rate Estimation

In general, the erosion rate of an ion-bombarded metal surface can be characterized by the energy of the impacting ion and the sputter yield, $S_{\alpha\beta}(\epsilon_\alpha)$, expressed in number of ejected atoms per incident ion. The yield is characteristic of the composition β of the metal surface, of the bombarding species α, and of the energy of the bombarding species ϵ_α. The rate of surface erosion R_β of species β by all species α is given by

$$R_\beta = \frac{A_\beta}{N_A \rho_\beta} \sum_\alpha \Gamma_\alpha S_{\alpha\beta}(\epsilon_\alpha) \qquad (1)$$

where N_A is Avogadro's number; ρ_β and A_β are the mass density and mass number of the metal β, respectively; and Γ_α is the incident flux of species α. Eq. (1) contains three implicit assumptions: 1) a constant angle is assumed for incidence of bombarding atoms onto the metal surface; 2) $S_{\alpha\beta}$ is assumed to be independent of Γ_α; and 3) the influence of the presence of one sputtering agent, α, on the yield $S_{\alpha'\beta}$ for another agent α' is assumed to be negligible (linearity assumption, generally valid at low current densities).

The species Hg^+ and Hg^{++} are the two principal sputtering agents‡ that are present in the discharge of a mercury ion thruster. Considering the bombarded surface to be Mo, Eq. (1) reduces to

$$R_{Mo} = \frac{A_{Mo}}{N_A \rho_{Mo}} [\Gamma_+ S(\epsilon_+) + \Gamma_{++} S(\epsilon_{++})] \qquad (2)$$

‡At least one other sputtering agent, Mo^+, is present in an ion thruster discharge. Molybdenum ions originate from sputtered Mo atoms which are ionized (with high probability) in the discharge plasma. Sputter erosion by Mo^+ is, however, a second-order process, since Mo^+ ions can only originate from atoms ejected by the first-order process, sputtering by mercury ions. In addition, the sputter yield of Mo^+ ions impacting a Mo surface is about 10^{-2} to 10^{-3}; therefore, Mo^+ bombardment does not result in erosion, but rather in net deposition on the bombarded surface.

A first-order calculation of expected sputter-erosion rates in a thruster discharge chamber consists of determining the incident fluxes Γ_+ and Γ_{++} and the energies ϵ_+ and ϵ_{++} for which appropriate yields S may be found. The energy of the ions impacting a surface is given by $\epsilon_\alpha = q_\alpha \Delta\phi$, where q_α is the species charge, and $\Delta\phi$ is the electrical potential difference between the surface being bombarded and the plasma potential where the ion was formed.

Equation (2) forms the basis for estimating molybdenum sputter-erosion rates R_{Mo}; this procedure is diagrammed in Fig. 5. Measurements are taken to provide the discharge computer model with the required input data. The model is used to produce maps of the bombardment fluxes Γ_+ and Γ_{++} to all surfaces. In addition, it produces maps of ion generation rates that can be used with plasma-potential data to calculate mean impact energies $\langle\epsilon_+\rangle$ and $\langle\epsilon_{++}\rangle$. These data are used with published sputter yields[9] S to calculate an estimated value for R_{Mo}.

Erosion rates have been estimated for surfaces in the SIT-8 thruster using the procedure just described; the results are presented in Table 2, where measured erosion rates (obtained by the LTF method described earlier) are shown for comparison. The predicted and observed erosion rates agree reasonably well, given the uncertainty which is expected to exist in published sputter yields (especially near threshold) and the errors introduced by the impact-energy averaging procedure.

The erosion-rate-estimation procedure has proven to be a valuable tool in investigating the parametric behavior of discharge-chamber sputter erosion. The accuracy of prediction inherent in this procedure has been found to be sufficient to investigate several thruster discharge phenomena.

Discussion

The results given in the preceding sections establish a data base and an analytical framework by which sputter-erosion processes in small mercury ion thrusters can be understood and predicted. Based on the foregoing discussion, one particularly important conclusion can be reached: the agent that produces the dominant portion of mass erosion in the discharge chambers of small mercury ion thrusters is the singly charged mercury ion, Hg^+. This conclusion is evident from the data presented in Table 2 and results simply from the very low relative population of doubly charged ions, which is indicated by the discharge computer model and confirmed by $E\times B$-type probe measurements of the ion beam. In larger thrusters (i.e., beam chamber $D_B \gtrsim 15$ cm), the doubly charged mercury ion density is typically higher.[10] This is particularly true near the center of the discharge chamber, far from recombination surfaces.

The dependence of dominant-sputtering species on thruster size can be approximately parameterized using a scaling rule for propellant utilization and the Hg^{++} generation-rate cross

Table 3 Summary of discharge-chamber erosion measurements

Location of laminar-film badge	Erosion rate, pm/h			
	SIT-8 standard configuration	SIT-8 revised configuration	SIT-12 standard configuration	SIT-12 revised configuration
Screen electrode				
Central region ($r \leq 8$ mm)	970-1450	610-920	971-1460	485-971
Outer region ($r > 8$ mm)	970-1450	310-610	971-1460	485-971
Screen polepiece				
Sharp edge	<490	310-610	971-1460	485-971
Elsewhere	<490	<310	<485	<485
Cathode-cup polepiece				
Inside	<490	<310	<485	<485
Downstream edge	2430-2920	610	4000-6000	<485
Ridge, downstream on outside	...	...	1943-2000	<485
Outside	<490	<310	<485	<485
Baffle				
Upstream	<970	...	<485	<485
Downstream	490-970	310-610	<485	<485-971 (narrow band near edge)
Endplate	<970	...	<485	<485
Total mass erosion rate, μg/h	81	25	144	60

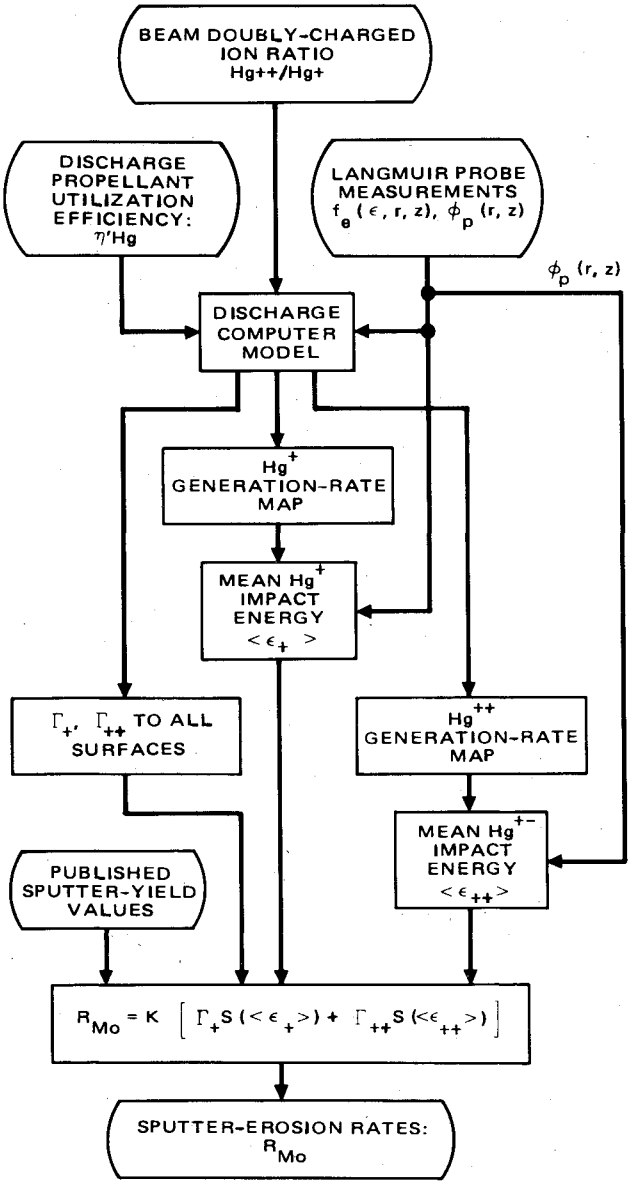

Fig. 5 Sputter-erosion rate estimation procedure.

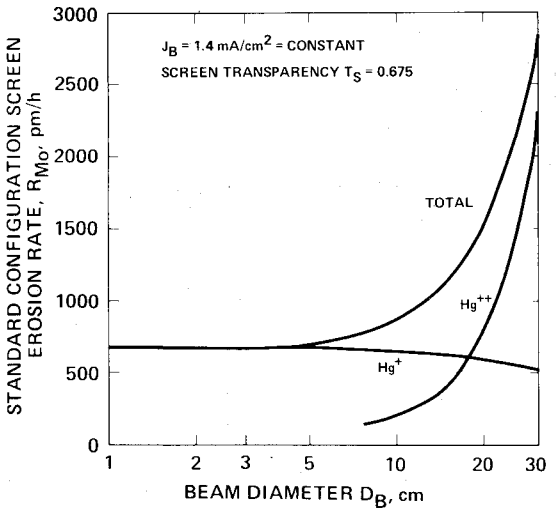

Fig. 6 Screen electrode erosion rate as a function of beam diameter for optimized SERT-II-type thrusters.

section. Calculations of this type have been carried out using available data for four optimized SERT-II-type thrusters (SIT-5, SIT-8, SIT-12, and 30 cm) to establish an approximate scaling law for sputter erosion. The rate of erosion of the screen electrode predicted by this model is plotted in Fig. 6 as a function of beam diameter D_B for SERT-II-type thrusters when operated at the same beam current density ($J_B = 1.4$ mA/cm^2). This semiempirical plot shows the erosion rate due to each ion species and the total erosion rate. The curve shown in Fig. 6 reflects the situation that Hg^{++} becomes the dominant sputtering agent for existing ion thrusters at a beam diameter somewhat above the value of $D_B = 12$ cm. Discharge-chamber sputter erosion, which has proven to be the principal life-limiting mechanism in 30-cm mercury ion thrusters, is clearly not life limiting for small thrusters.

Reduction in Erosion Rate

Several approaches to reducing the rate of discharge-chamber sputter erosion are suggested by the identification of sputter-erosion mechanisms and patterns and the scaling behavior described earlier. In small thrusters, where erosion of the screen electrode by Hg^+ dominates, sputter erosion can

be reduced by lowering the impact energy of bombarding ions. This approach has been investigated in the SIT-8 and SIT-12 thrusters by biasing the thruster shell (including screen electrode) at keeper potential (rather than at cathode potential as in conventional SIT-8 design operation) and reducing the discharge voltage from $V_D = 40$ V to $V_D = 37.5$ V. As shown in Table 3, these changes reduced by threefold the rate of total discharge-chamber mass erosion. No significant performance penalty was incurred by this modification.

In larger thrusters, where Hg^{++} is the dominant sputtering agent, the Hg^{++} generation rate can be reduced by raising the neutral-mercury density in the discharge plasma. This, of course, means reducing the propellant utilization efficiency.§

Conclusions

The processes of discharge-chamber sputter erosion have been studied in small mercury ion thrusters using direct LTF measurements of the erosion rates and a correlated program of plasma measurements and modeling to interpret the erosion-rate data. The principal findings of the investigation are listed below:

1) In small thrusters, Hg^{+} is the dominant sputtering agent.

2) In small thrusters, the screen electrode is the surface that experiences the greatest amount of mass erosion. Erosion of the screen electrode is remarkably uniform.

3) A threefold reduction in discharge-chamber mass erosion rate has been demonstrated in small thrusters by operating the thruster with the shell maintained at keeper potential and reducing the discharge voltage from $V_D = 40$ V to $V_D = 37.5$V.

4) In larger thrusters, Hg^{++} is the dominant sputtering agent; Hg^{++} generation is primarily a function of the Hg^0 to Hg^{+} density ratio, n_0/n_+, and is only weakly dependent on discharge voltage.

5) Discharge-chamber sputter erosion is not life threatening for small thrusters and is readily dealt with by existing sputter-control methods.

§Loss of propellant utilization due to increased neutral density can be avoided to some extent by reducing the accel transparency (i.e., reducing the neutral-loss open area) as in the use of an ion-machined extraction system.[11]

Acknowledgments

Special acknowledgment is due H. L. Garvin who developed the required techniques for deposition of multilayer films on sample surfaces and invented the diagnostic-etch procedure, which was essential to the success of the subject investigation. This paper is based on work performed under the sponsorship of the International Telecommunications Satellite Organization (INTELSAT). Any views expressed are not necessarily those of INTELSAT.

References

[1] Power, J. L., "Sputter Erosion and Deposition in the Discharge Chamber of a Small Mercury Ion Thruster," AIAA Paper 73-1109, AIAA 10th Electric Propulsion Conference, Lake Tahoe, Nev., Oct. 31-Nov. 2, 1973.

[2] Collett, C. R. and Poeschel, R. L., "A 10,000-h Endurance Test of a 700 Series 30-cm Engineering Model Thruster," AIAA Paper 76-1019, AIAA 12th Electric Propulsion Conference, Key Biscayne, Fla., Nov. 1976.

[3] Power, J. L. and Hinzay, D. J., "Solutions for Discharge-Chamber Sputtering and Anode Deposit Spalling in Small Mercury Ion Thrusters," NASA TMX-71675, 1975.

[4] Free, B. A., Meadows, G. A., and Morell, N., "Effect of a Decel Electrode on Charge Exchange Erosion Pattern in an Ion Thruster," presented at Third European Electric Propulsion Conference, Hinterzarten, Black Forest, Federal Republic of Germany, Oct. 14-18, 1974.

[5] Ward, J. W. and Masek, T. D., "A Discharge Model for an Electron Bombardment Thruster," AIAA Paper 76-1009, AIAA 12th Electric Propulsion Conference, Key Biscayne, Fla., Nov. 1976.

[6] Hyman, J., Jr., Dulgeroff, C. R., Kami, S., and Williamson, W. S., "One-Millipound Mercury Thruster," *Journal of Spacecraft and Rockets*, Vol. 13, June 1976, pp. 366.

[7] Hyman, J., Jr. and Dulgeroff, C. R., "Modularized Ion Thruster Development," AIAA Paper 76-1049, AIAA 12th Electric Propulsion Conference, Key Biscayne, Fla., Nov. 1976.

[8] Strickfaden, W. B. and Geiler, W. L., "Probe Measurements of the Discharge in an Operating Electron Bombardment Engine," Jet Propulsion Laboratory, Pasadena, Calif., TR 32-417, April 19, 1964; also *AIAA Journal*, Vol. 7, Aug. 1963, pp. 1815-1823.

[9] Askerov, Sh. G. and Sena, L. A., "Cathode Sputtering of Metals by Slow Mercury Ions," *Soviet Physics-Solid State*, Vol. 11, Dec. 1969, p. 1288.

[10] Kaufman, H. R., and Cohen, A. J., "Maximum Propellant Utilization in an Electron Bombardment Ion Thruster," Symposium on Ion Sources and Ion Beams, Brookhaven National Laboratory, 1971.

[11] Hudson, W. R. and Banks, B. A., "Ion Machined Accelerator Grid Tests," NASA TMX-71611, 1974, p. 24.

Announcement: 1978 Author and Subject Index

The indexes of the six AIAA archive journals (*AIAA Journal, Journal of Aircraft, Journal of Energy, Journal of Guidance and Control, Journal of Hydronautics, Journal of Spacecraft and Rockets*) will be combined and mailed separately early in 1979. In addition, papers appearing in volumes of the *Progress in Astronautics and Aeronautics* book series published in 1978 will be included. Librarians will receive one copy of the index for each subscription which they have. Any AIAA member who subscribes to one or more Journals will receive one index. Additional copies may be purchased by anyone, at $10 per copy, from the Circulation Department, AIAA, Room 730, 1290 Avenue of the Americas, New York, New York 10019. **Remittance must accompany the order.**

Ruth F. Bryans
Administrator, Scientific Publications